

Article

Antireflection Improvement and Junction Quality Optimization of Si/PEDOT:PSS Solar Cell with the Introduction of Dopamine@Graphene

Tao Chen ^{1,2} , Hao Guo ², Leiming Yu ^{1,2}, Tao Sun ², Anran Chen ², Juan Wang ², Chong Wang ² and Yu Yang ^{2,*}

¹ School of Physics and Astronomy, Yunnan University, Kunming 650091, China; taochen008@ynu.edu.cn (T.C.); yuleiming@mail.ynu.edu.cn (L.Y.)

² International Joint Research Center for Optoelectronic and Energy Materials, School of Materials and Energy, Yunnan University, Kunming 650091, China; guohao2408@mail.ynu.edu.cn (H.G.); t.sun@griffith.edu.au (T.S.); 20170027@ynu.edu.cn (A.C.); wjuan0130@ynu.edu.cn (J.W.); cwang@ynu.edu.cn (C.W.)

* Correspondence: yuyang@ynu.edu.cn

Received: 18 October 2020; Accepted: 12 November 2020; Published: 16 November 2020



Abstract: Si/PEDOT:PSS solar cell is an optional photovoltaic device owing to its promising high photovoltaic conversion efficiency (PCE) and economic manufacture process. In this work, dopamine@graphene was firstly introduced between the silicon substrate and PEDOT:PSS film for Si/PEDOT:PSS solar cell. The dopamine@graphene was proved to be effective in improving the PCE, and the influence of mechanical properties of dopamine@graphene on solar cell performance was revealed. When dopamine@graphene was incorporated into the cell preparation, the antireflection ability of the cell was enhanced within the wavelength range of 300~450 and 650~1100 nm. The enhanced antireflection ability would benefit amount of the photon-generated carriers. The electrochemical impedance spectra test revealed that the introduction of dopamine@graphene could facilitate the separation of carriers and improve the junction quality. Thus, the short-circuit current density and fill factor were both promoted, which led to the improved PCE. Meanwhile, the influence of graphene concentration on device performances was also investigated. The photovoltaic conversion efficiency would be promoted from 11.06% to 13.15% when dopamine@graphene solution with concentration 1.5 mg/mL was applied. The achievements of this study showed that the dopamine@graphene composites could be an useful materials for high-performance Si/PEDOT:PSS solar cells.

Keywords: dopamine@graphene; Si/PEDOT:PSS solar cell; junction quality; antireflection

1. Introduction

Solar energy holds a great potential for compensating the energy shortage. The silicon/poly(3,4-ethylenedioxy-thiophene):poly(styrene-sulfonate) (Si/PEDOT:PSS) solar cell possesses advantageous of organic and nonorganic materials with low cost and easy processing [1]. The interface contact between Si and PEDOT:PSS film, conductivity of PEDOT:PSS film, and reflectance property of the cell have essential influence on the further improvement of photovoltaic conversion efficiency (PCE) [2,3]. Thus, much efforts for improving the PCE of solar cell have been performed [4–7]. The PCE of Si/PEDOT:PSS solar cell have already exceeded 17% since it was born [8], and still exhibited great potential for further improvement [5,9,10].

For Si/PEDOT:PSS solar cell, the electron-hole pairs are generated in Si substrate, and PEDOT:PSS film is mainly responsible for blocking the electrons, transporting the hole to electrode, and acting

as surface passivation and antireflection layer [11]. Thus, the optical and electrical properties of PEDOT:PSS film are important for the PCE enhancement of cell. Doping modification for PEDOT:PSS solution is a simple and cost-effective method to modify the optical and electrical properties. The most popular modification methods were solvent treatment [6,12–14] and addition of nanomaterials [15–17]. Considering the bare Si substrate was directly covered by PEDOT:PSS film for original cell structure, two major problems are introduced, i.e., the defects on Si surface are not passivated and the interface contact between PEDOT:PSS film and Si substrate is poor [18]. To solve the problems, a thin interface layer was introduced. Silicon oxide (SiO_x) [19,20], aluminum oxide (Al_2O_3) [13], and titanium oxide (TiO_x) [21] were prepared on the Si surface. Oxide passivation layer showed effectiveness in reducing the surface state density of bare Si substrate. In this way, the defects on the Si surface was minimized, and the carrier separation was also facilitated. These influences would improve the interface contact and junction quality of solar cell. However, the complex and high-cost synthesis or preparation procedure of oxide layer will limit its application. Thus, layer with low cost and easy preparation was proposed. Liu et al. [22] improved the cell performance by inserting an ultrathin ferroelectric poly(vinylidene fluoridetetrafluoroethylene) P(VDF-TeFE) layer into the PEDOT:PSS film and Si interface. Liu et al. [23] inserted a layer of 1, 4, 5, 8, 9, 11-hexaazatriphenylene hexacarbonitrile (HAT-CN) into the cell, and the V_{bi} and Φ_b was strengthened by the formation of a quasi p–n junction. Zhu et al. [24] prepared a 35 nm layer with PEDOT:PSS (AL 4083) on Si substrate as an interface layer, and the cell performance was improved. These results indicated that introduction of interface layer for Si/PEDOT:PSS solar cell is a promising method for improving the PCE of solar cell.

Graphene has been applied in the nanoelectronics, solar cells, batteries, and super capacitors owing to its desired light transparency, high electrical conductivity, and large specific surface area. In last years, the graphene dispersed in PEDOT:PSS has been applied into Si/PEDOT:PSS solar cell [15,17,25]. The graphene in PEDOT:PSS film would contribute to reducing the reflection and decreasing the sheet resistance of the composites film. Although the addition of graphene into PEDOT:PSS solution is an easy and low-cost way for benefitting the cell performance improvement, the less amount of graphene in PEDOT:PSS could not form the conductivity network. When the amount of graphene in PEDOT:PSS solution was increased, the well dispersion of graphene was hard to achieved and the aggregation of graphene would affect the optical performance of the composites film. Thus, it is necessary to develop a method to prepare the graphene network with reasonable amount and desired optical property.

The chemical vapor deposition (CVD) is a universal method to prepare the graphene film with desired optical performance for photovoltaic application [26–28]. Although the optical and electrical performance of graphene film is desired and useful for the performance enhancement of photovoltaic device, the CVD process and graphene film transferring were relatively complicated and uneconomical. Dopamine (DA) is a nontoxic organic material and can self-polymerize into highly adhesives poly(dopamine) (PDA), which hold π – π stacking interactions structures [29,30]. Besides, Hu et al. [31] and Qin et al. [32] demonstrated that the DA could benefit the dispersion of graphene and prevent the aggregation. The dopamine has been applied in perovskite solar cells and exhibits great potential as hole transport material [33–36]. While, the application of dopamine in Si/PEDOT:PSS solar cell has not been reported yet.

In this investigation, the dopamine@graphene (DA@G) composite was introduced into the Si/PEDOT:PSS solar cell to improve the cell performance. It could be found that the short-circuit current density (J_{sc}) and fill factor (FF) of the prepared DA@G incorporated solar cell were improved. The optimal solar cell showed a PCE of 13.15% with J_{sc} of 32.64 mA/cm^2 , open-circuit voltage (V_{oc}) of 623 mV, and FF of 64.64%. The chemical structure and micromorphology of DA@G composites were studied. The morphology and performance of DA@G coated on Si substrate were also considered. The effect of DA@G on the junction quality of solar cell was presented under the assistant of electrochemical impedance spectra (EIS) measurement. The influence of graphene concentration on solar cell performances was also presented. This research introduced the DA@G composites to realize

the preparation of high-performance Si/PEDOT:PSS solar cell for the first time. The achievements of this study exhibited that the DA@G composites had a great potential for improving the performance of Si/PEDOT:PSS solar cell.

2. Materials and Methods

2.1. Materials

One-side polished n-silicon wafers with resistivity of 0.05–0.1 Ω -cm and thickness of 300 μ m were purchased from Hefei-Kejing Materials Technology Co., Ltd. (Hefei, China). PEDOT:PSS (Clevios PH1000, Heraeus, Hanau, Germany) aqueous solution was purchased from Sigma-Aldrich (Shanghai, China). Phenyl-C61-butyric acid methyl ester (PC61BM, >99.5%) was supplied by Xi'an Polymer Light Technology (Xi'an, China). Dimethyl sulfoxide (DMSO, 99.9%), dopamine hydrochloride (98%), ethanol, sulfuric acid (H_2SO_4 , AR, 98%), hydrochloric acid (HCl, AR, 36%), acetone, hydrogen peroxide (H_2O_2 , AR, 30 wt% in H_2O), and hydrofluoric acid (HF, AR, $\geq 40\%$) were purchased from Yunnan-Keyi (Kunming, China). Tris(hydroxymethyl)aminomethane (Tris) and graphene (>95%) were purchased from Shanghai Aladdin Biochemical Technology Co., Ltd. (Shanghai, China).

2.2. Experiment and Device Preparation

DA@G solution preparation: G with different weight (1, 2, 3, and 4 mg) was dispersed in 2 mL deionized (DI) water under ultrasonic treatment (20 min). Tris was added into the G solution, and the solution PH was adjusted to 8.5 with HCl solution. Further, 2 mg DA was added into the solution and stirred for 24 h under ambient temperature. Besides, the DA solution was also prepared i.e., 2 mg DA was added in to DI water, with pH = 8.5, and stirred for 24 h.

Solar cell preparation: The silicon wafer was cut into square substrates with dimensions of 10 mm \times 10 mm. As illustrated in Figure 1, silicon substrates were cleaned according the RCA method, and transferred into glove box immediately after nitrogen drying. The DA and DA@G solution was spinning coated on the front (polished) side of substrate with speed of 4000 rpm and time of 30 s, then dried at 130 $^{\circ}$ C for 20 min. After cooled to the ambient temperature, the PEDOT:PSS solution (doped with 5 wt.% DMSO and 0.2 wt.% Triton X-100) was spinning coated with speed of 4000 rpm and time of 60 s. After drying at 130 $^{\circ}$ C for 20 min, it was cooled to ambient temperature; the PC61BM (20 mg/mL) was spin-coated on the rear side of the substrate with speed of 2000 rpm and time of 40 s. The PC61BM film could help facilitating the electron collection. After drying at 80 $^{\circ}$ C for 10 min and cooling to ambient temperature, the substrate was coated with PEDOT:PSS film; then, DA@G and PC61BM film was put into vacuum evaporating instrument to prepare 200 nm silver (Ag) grid and 100 nm aluminum (Al) film. For each experiment set, 10 samples were prepared.

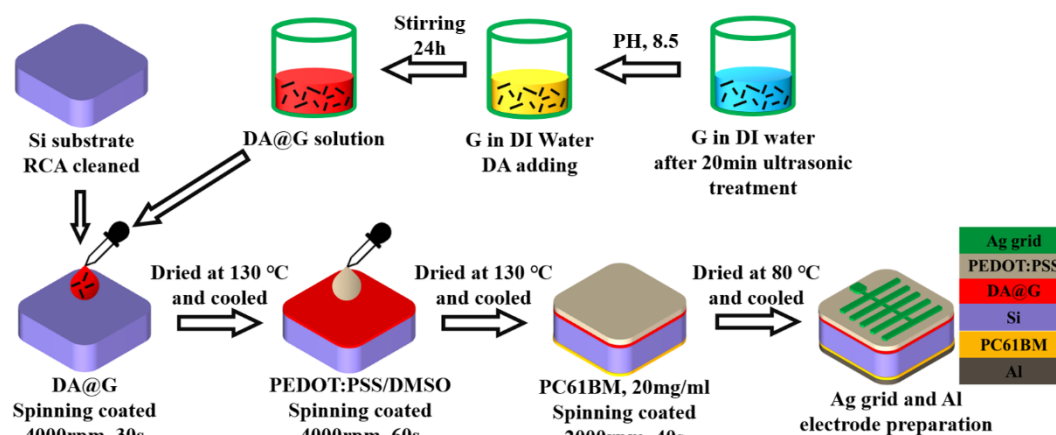


Figure 1. Preparation process for dopamine@graphene (DA@G) solution and solar cell.

2.3. Characterizations

Keithley 2400 (Tektronix Inc., Beaverton, OR, USA) under the simulated solar illumination (AM 1.5 Global solar simulator) with intensity 100 mW/cm^2 (calibrated by a standard monocrystalline silicon solar cell) was applied to measure the current density–voltage (J–V) curve of solar cells. The EIS measurement was performed via an electrochemical workstation (Model 660D, Shanghai Chen Hua Instrument Co., Ltd., Shanghai, China). The transmittance and reflectance were measured by spectrophotometer (UV-3600Plus, Shimadzu, Kyoto, Japan), and the wavelength ranged from 200 to 1200 nm. Transmission electron microscope (TEM, JEM-2100, JEOL Ltd., Akishima, Japan) and scanning electron microscope (SEM, Nova NanoSEM 450, FEI, Hillsboro, OR, USA) characterizations were applied to analyze the morphology. Fourier-transform infrared spectrometer (FTIR, Nicolet iS10, Thermo Fish Scientific, Waltham, MA, USA) and X-ray photoelectron spectroscopy (XPS, K-Alpha+, Thermo Fish Scientific, Waltham, MA, USA) were used for the chemical structure analyzation of DA@G. External quantum efficiency (EQE) measurements were performed with a quantum efficiency measurement system (SCS10, Zolix, Beijing, China).

3. Results

The FTIR analysis was applied to obtain the surface chemical information of G and DA@G3 powder. Figure 2a presented FTIR spectra of G and DA@G3 powder. In Figure 2a, the FTIR spectra of G powder illustrated two major absorption peaks at 3436 cm^{-1} (OH stretching vibration) and 1624 cm^{-1} (C=C stretching vibration). The peaks at 1725 cm^{-1} (C=O stretching vibrations) and 1060 cm^{-1} (C–O (alkoxy) stretching vibration) were not observed. The absence of such peaks stated that the defects of G sheet was greatly depressed, and the G powder had desired performances. When G was coated with DA, a wide peak at 1120 cm^{-1} were observed according to the FTIR spectra of DA@G3 powder. This peak could be owing to the immersion of C–N stretching vibration at 1040 cm^{-1} and phenolic C–OH stretching vibration at 1211 cm^{-1} [37,38]. Meanwhile, the peaks at 3436 and 1624 cm^{-1} became much more deep, which was resulted from N–H stretching vibration around 3436 cm^{-1} and N–H bending vibration around 1624 cm^{-1} . The N–H stretching vibration and N–H bending vibration were introduced by DA. The amide (II) vibration was also immersed within the peak at 1624 cm^{-1} [39].

XPS analysis was also performed on G and DA@G3 powder to gain further information about the chemical composition. In Figure 2b, the core levels of C1s and O1s locating at 284.8 and 532.1 eV were recorded for G powder. As for the DA@G3 powder, the C1s at 284.8 and O1s at 532.1 eV were recorded. Besides, core levels for nitrogen (N1s) was observed around 400 eV owing to incorporation of DA. The high-resolution scans for C1s was presented in Figure 2c. The variations of C1s signal between G and DA@G3 powder were very small, stating that DA had little effect on the main structure of G. The effect of C–N group on the C1s was not clear. This might be owing to the very small amount of DA coated on the G, which made it hard to be detected. In Figure 2d, the high-resolution scans of N1s could be fitted into three components. The peaks located at 398.5, 400.2, and 402 eV corresponded to –NH=, –NH–, and –NH₂, respectively [38]. These XPS analysis revealed that DA have been successfully coated onto the G surface through the oxidative polymerization [40].

The microstructure of G and DA@G3 powder was characterized by the SEM and TEM. The SEM images in Figure 3a illustrated that G powder exhibited a typical aggregated morphology, and the aggregation of DA@G3 powder was greatly depressed as illustrated in Figure 3b. Thus, the DA was helpful in facilitating the G dispersion. The thickness of G sheet in Figure 3c was much thicker than that in Figure 3d. The transparent and corrugated sheet appeared in Figure 3d indicating that the DA could contribute to the exfoliation of G.

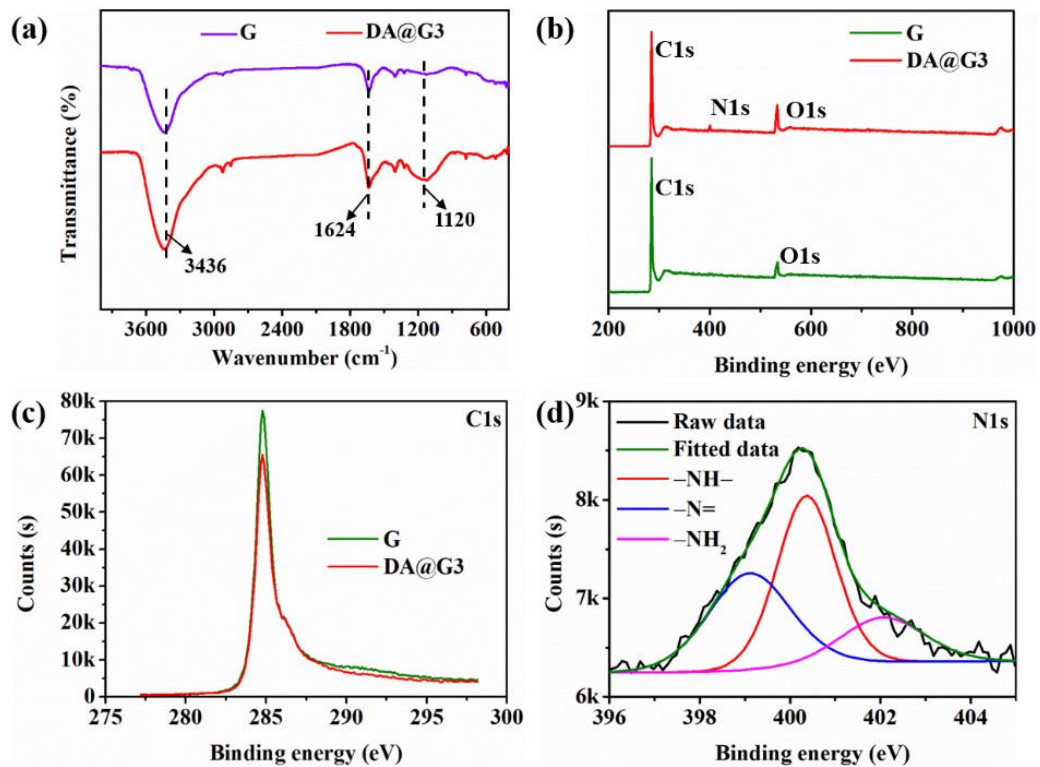


Figure 2. FTIR and XPS spectra for G and DA@G3 powder: (a) FTIR spectra, (b) XPS survey scan, (c) high resolution scans for C1s, and (d) high-resolution scans for N1s.

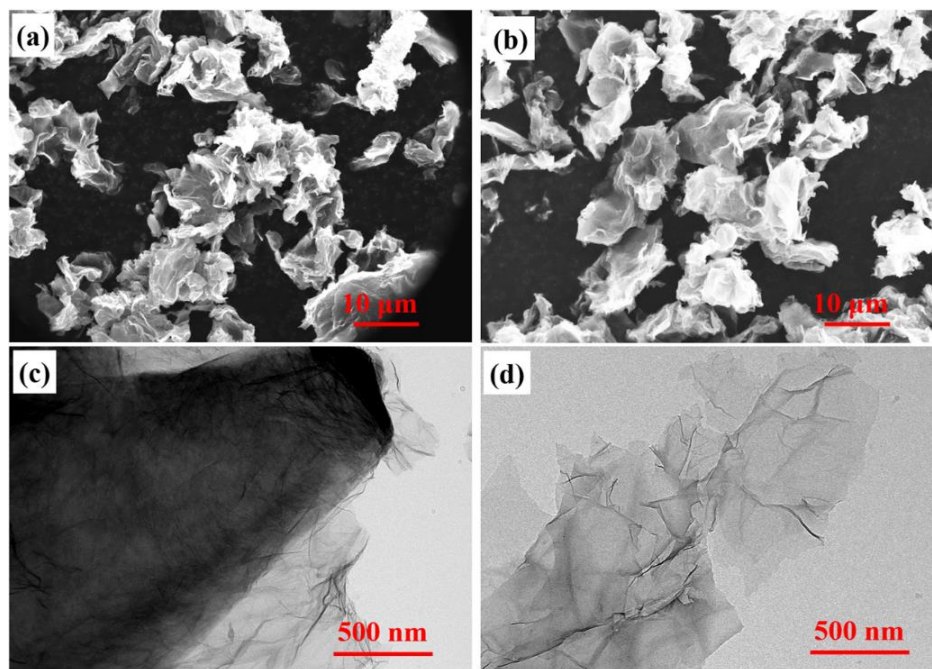


Figure 3. The SEM and TEM images for G and DA@G powder: (a) and (c) for G and (b) and (d) for DA@G.

The prepared DA@G composites according to Figure 1 were applied to prepare the solar cell. The J–V curves under illumination of AM 1.5 G light and dark are presented in Figure 4. The performance parameters of prepared solar cell (the most optimal) are summarized in Table 1. As illustrated in Table 1, the pristine cell (without DA and DA@G introduced) had a PCE of 11.06% with J_{sc} of 30.87 mA/cm²,

V_{oc} of 628 mV, and FF of 57.08%. When DA was introduced into the solar cell, the PCE of solar cell was improved to 11.43% with enhanced J_{sc} and FF. The highest PCE of solar cell was obtained when DA@G3 was involved into the cell preparation, and the PCE was 13.15% with J_{sc} of 32.64 mA/cm², V_{oc} of 623 mV, and FF of 64.64%. The J_{sc} and FF could also be improved when compared with the solar cell just incorporated with DA.

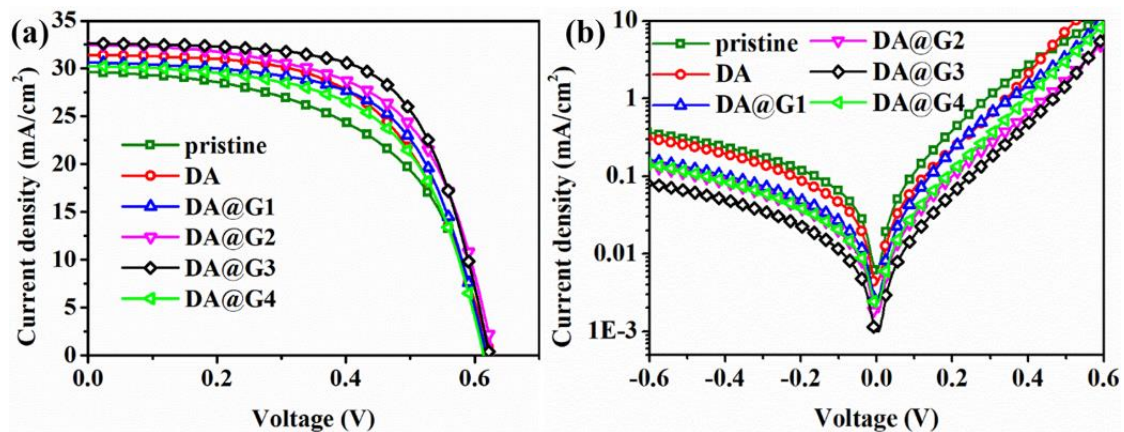


Figure 4. Current density–voltage (J–V) curves of prepared solar cells with different G concentration: (a) under illumination of AM 1.5 G light and (b) under dark condition.

Table 1. Performance parameters of the most optimal solar cell.

Performance Parameter	PCE (%)	V_{oc} (mV)	J_{sc} (mA/cm ²)	FF (%)
Pristine	11.06	628	30.87	57.08
DA	11.43	626	31.43	58.13
DA@G1	11.71	627	31.43	59.99
DA@G2	12.52	629	32.47	61.32
DA@G3	13.15	623	32.64	64.64
DA@G4	11.06	614	30.27	59.48

Performance parameters of prepared solar cells would change with G concentration varying as Table 1 illustrating. Thus, the parameters of tested solar cells for each experiment set are presented in Figure 5. PCE of prepared cells was improved with increased G concentration until the concentration reached 1.5 mg/mL (DA@G3). When the G concentration was increased to 2 mg/mL (DA@G4), the PCE was dropped obviously. The FF and J_{sc} of solar cell both showed the same evolution trend as PCE when G concentration varied. In Figure 5d, the V_{oc} of solar cell was nearly unchanged when G concentration was increased to 1 mg/mL (DA@G2). When G concentration was further increased to 2 mg/mL (DA@G4), the V_{oc} was decreased. These results revealed that the G concentration could greatly affect the performance of prepared solar cell. The improved PCE of solar cells was mainly owed to the enhancement of FF and J_{sc} . To give reasonable explanation for cell performance changing with G concentration, further investigation was presented in next.

Considering that the DA@G was introduced into PEDOT:PSS/Si solar cell between the PEDOT:PSS film and Si substrate, it is important to understand the optical transmittance property of DA@G. The DA@G was spin-coated onto the silica glass surface. The optical transmittance spectra is illustrated in Figure 6a. The optical transmittance of silica glass was slightly higher than 90%. When DA@G were coated onto silica glass surface, the transmittance was further decreased with increasing G concentration. The silica glass covered with DA@G3 showed an acceptable optical transmittance of around 78%. As for the silica glass covered with DA@G4, the optical transmittance was decreased to 62%. Such low optical transmittance would restrict the light utilization for solar cell and led to the reduction in cell performances, including PCE, J_{sc} , V_{oc} , and FF as illustrated in Figure 5.

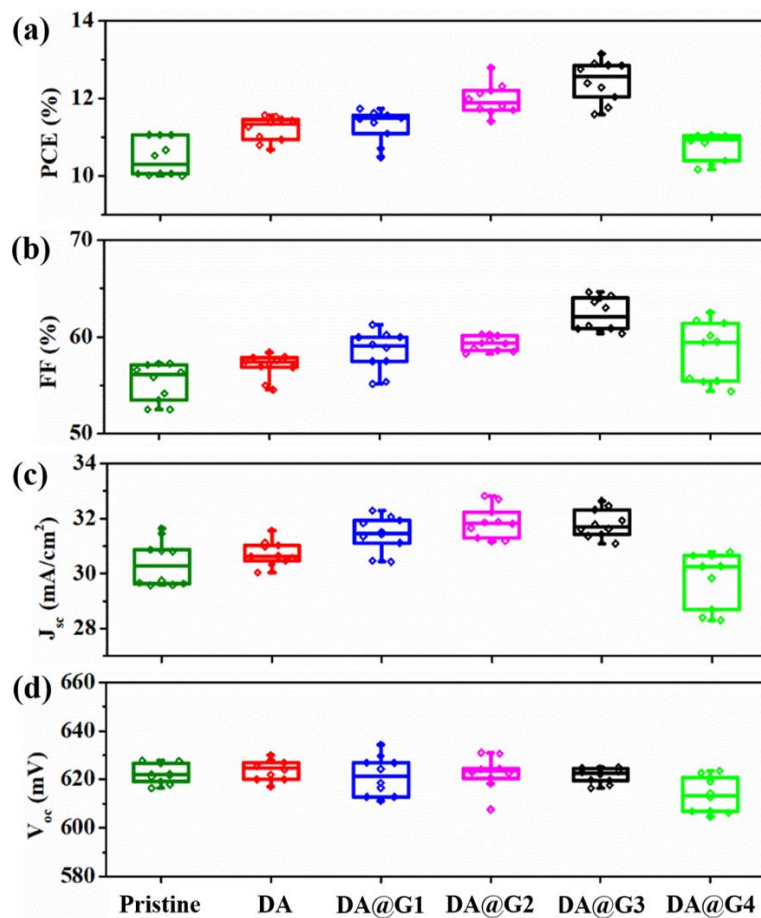


Figure 5. Performance parameters of prepared solar cells versus G concentration: (a) photovoltaic conversion efficiency (PCE), (b) fill factor (FF), (c) short-circuit current density (J_{sc}); (d) open-circuit voltage (V_{oc}).

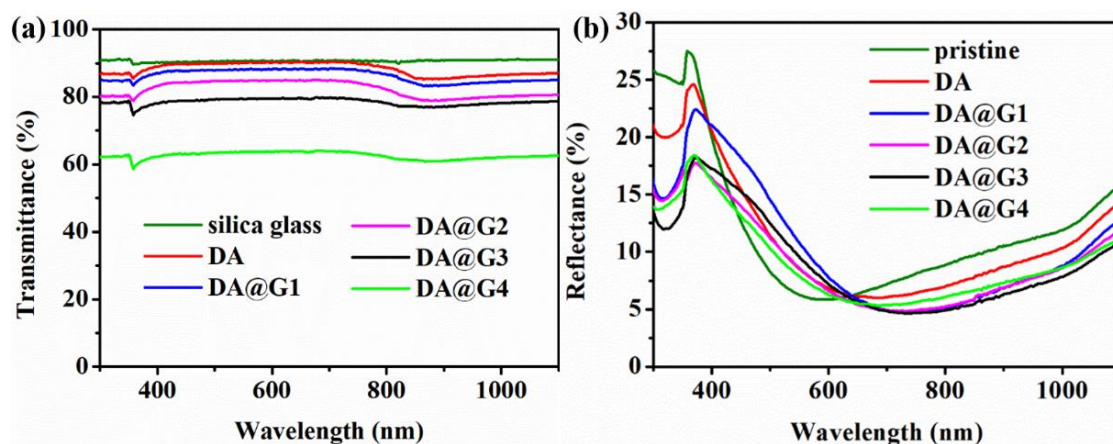


Figure 6. Transmittance and reflectance spectra. (a) Optical transmittance spectra of silica glass and DA@G spinning coated on silica glass and (b) reflectance spectra of PEDOT:PSS/Si (pristine), PEDOT:PSS/DA/Si (DA), and PEDOT:PSS/DA@G/Si.

Apart from the transmittance, the reflectance also played an important role in affecting the performance of solar cell. Samples of the PEDOT:PSS/Si (pristine), PEDOT:PSS/DA/Si (DA), and PEDOT:PSS/DA@G/Si were prepared without Ag grid covering for reflectance measurement. The reflectance spectra for different samples are illustrated in Figure 6b. The introduction of DA@G would lead to the lower reflectance spectra in two wavelength regions than the pristine samples. The two

regions were 300~450 and 650~1100 nm as showed in Figure 6b. Besides, the sample incorporated with DA@G3 had the lowest reflectance spectra in these regions, indicating the optimal antireflection ability. The lower reflectance could lead to more photogenerated carriers in Si substrate [15,41]. External quantum efficiency (EQE) spectra results in Figure 7 showed a very good agreement with the reflectance spectra, which further stated that the carrier separation and the light utilization was much efficient when DA@G3 was introduced. Therefore, the enhancement of J_{sc} should be partially ascribed to the antireflection effect of DA@G.

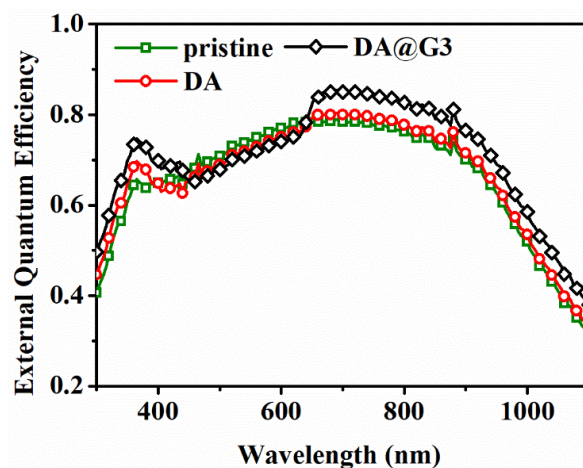


Figure 7. External quantum efficiency (EQE) spectra for solar cells without DA@G (pristine), with dopamine (DA) and with DA@G3.

SEM images for the morphology of DA@G coated on the Si substrate are presented in Figure 8a–e, and the insert images are the images with high magnification. When G concentration was increased, the amount of G coated on Si substrate became larger as presented in Figure 8, which would promote the charge carriers conduct in the DA@G composites [15]. While, the aggregation of G also occurred with the increasing G concentration, which would restrict the optical transmittance of DA@G as stated in Figure 6a. In Figure 8e, the aggregation phenomenon became very serious compared with other samples. When DA was coated on the Si substrate, the uncontinuous structure with lots of holes were formed as shown in Figure 8a. In Figure 8b, the uncontinuous structure was observed from the insert images. Similar structure also occurred in the samples with DA@G1, DA@G2, and DA@G4. In Figure 8d, the insert image stated that the holes disappeared, and an intact film was formed on Si substrate. These images proved that the introduction of DA@G could facilitate the formation of an intact film on the Si substrate. The intact film in Figure 8d indicated that the DA@G3 composites covered the Si substrate very well, which would benefit the improved interface contact and junction quality. In Figure 8f,g, the cross-section SEM images of PEDOT:PSS/Si and PEDOT:PSS/DA@G3/Si are presented. The PEDOT:PSS film was very neat and flat as shown in Figure 8f. The interface between PEDOT:PSS and DA@G3 was hard to distinct in Figure 8g. This was owed to the hydrophilic poly(dopamine) coated on G, which could facilitate the interface adhesion between PEDOT:PSS and DA@G. Besides, the PEDOT:PSS/DA@G3 illustrated a much better interface contact with Si substrates than single PEDOT:PSS. The SEM characterization results proved that the introduction of DA@G3 would benefit the intact film formation on Si substrate and better interface contact with Si substrate. Such benefits might contribute to the junction quality improvement of prepared solar cell.

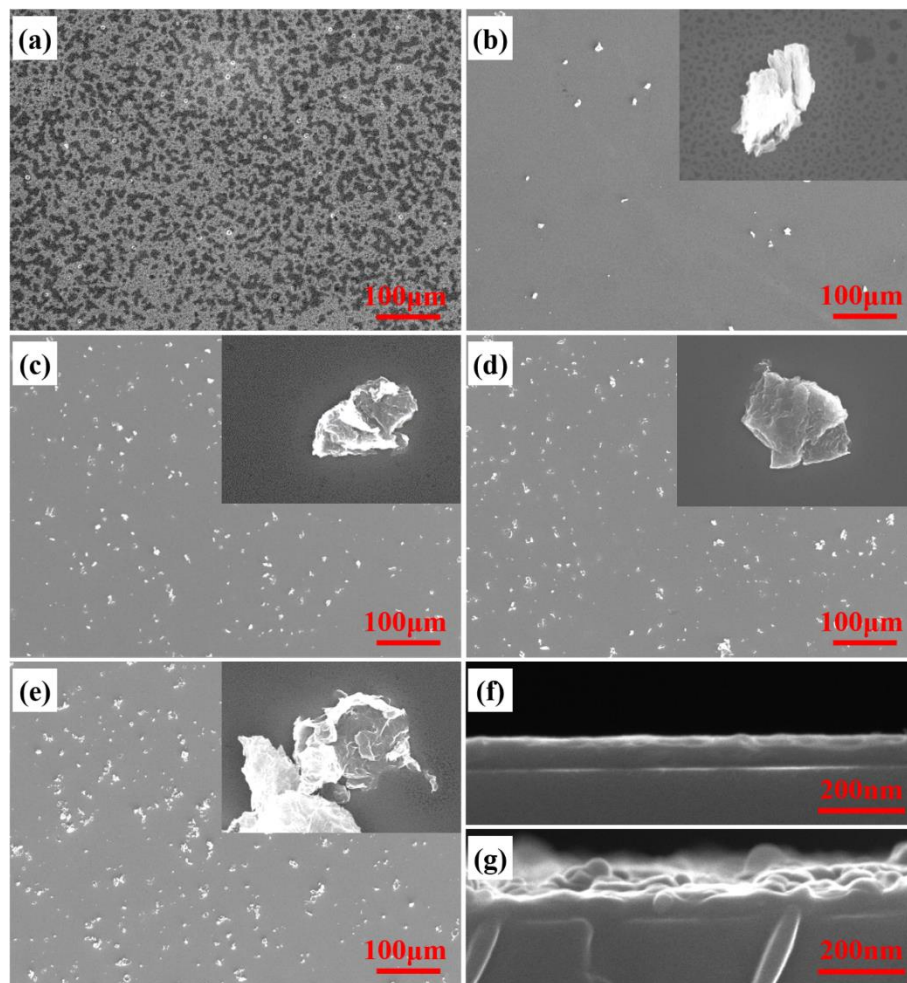


Figure 8. SEM images for front surface of (a) DA/Si, (b) DA@G1/Si, (c) DA@G2/Si, (d) DA@G3/Si, and (e) DA@G4/Si and the inserts were the images with high magnification. SEM images for cross-section of (f) PEDOT:PSS/Si and (g) PEDOT:PSS/DA@G3/Si.

To further investigate the junction quality, the measured and fitted Nyquist plots of different solar cells with EIS testing are presented in Figure 9. The equivalent circuit model (R_s : series resistance, R_{rec} : recombination resistance, and C_1 : junction capacitance) for the spectra fitting is also presented in Figure 9. The spectra for different solar cells were nearly semicircular, stating that only a single junction formed in prepared solar cell. The spectra heights and diameters of solar cells rose with increasing G concentration until the concentration reached 1.5 mg/mL (DA@G3), and then decreased when concentration was 2 mg/mL (DA@G4). Such revolution was related to the recombination resistance (R_{rec}) and the junction capacitance (C_1). To give a full understanding about the EIS testing results, the data were fitted with an equivalent circuit model. The model was composed of a parallel connected R_{rec} - C_1 and a series resistance (R_s). Table 2 illustrated the fitted parameters. It could be seen that R_s showed a decrease until G concentration reached 1.5 mg/mL (DA@G3), then increased when concentration was 2 mg/mL (DA@G4). While, the R_{rec} exhibited the opposite evolution trend with G concentration. The R_{rec} was a key parameter affecting the cell performance, because high R_{rec} could depress the carrier recombination and suppress the leakage current at the junction. Lower R_s revealed that the drift current at the junction was suppressed under dark conditions, and the reverse saturation current was also minimized. For solar cells, the dark current was composed of reverse saturation current and leakage current. The dark current could be minimized with lower R_s and increased R_{rec} (as illustrated in Figure 4b). The minimized dark current meant the carrier recombination was suppressed. In another words, the reduced R_s and increased R_{rec} revealed that the

high-quality junction was formed at the interface. The minor carrier lifetime (τ) was obtained based on the relationship between R_{rec} and C_1 [42]. The results were listed in Table 2. High τ indicated that carrier separation was encouraged at the interface. The solar cell incorporated with DA@G3 showed the lowest R_s and highest R_{rec} and τ . The solar cell incorporated with DA@G3 had the most optimal junction quality, which would benefit the performance improvement of solar cell, especially the FF.

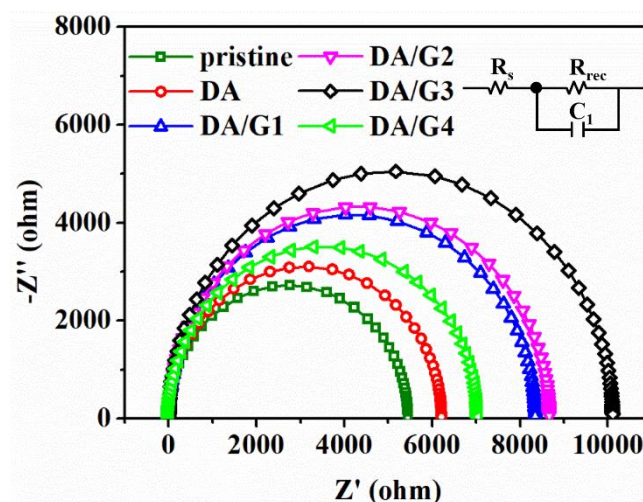


Figure 9. Nyquist plots obtained from the electrochemical impedance spectra: the scatters were the experiment data and the solid lines were the fitted.

Table 2. Impedance characteristics of the tested devices.

Characteristic	R_s (ohm)	R_{rec} (ohm)	C_1 (F)	τ (μ s)
Pristine	3.45	5445	1.34×10^{-7}	731.5
DA	3.29	6211	1.34×10^{-7}	831.8
DA@G1	3.25	8342	1.26×10^{-7}	1059.4
DA@G2	2.86	8662	1.27×10^{-7}	1095.6
DA@G3	2.80	10370	1.32×10^{-7}	1365.7
DA@G4	3.06	7037	1.30×10^{-7}	914.3

4. Conclusions

This study firstly proved that the performance of PEDOT:PSS/Si solar cell could be improved through the introduction of DA@G composites. The introduction of DA@G composites could reduce the reflectance of the cell within the wavelength range of 300~450 and 650~1100 nm. The reduced reflectance meant more photons could be converted to charge carriers. The introduced DA@G composites could also contribute to improving the junction quality through suppressing the leakage current and facilitating the carrier separation. Thus, the enhanced antireflection ability could help producing more charge carriers, and the optimized junction quality could promote the carrier separation. In this way, the J_{sc} and FF of prepared solar cell were improved. The graphene concentration in DA@G composites could affect the performances of solar cell because the reflectance and junction quality of solar cell were varied with the changing graphene concentration. The most optimal solar cell with PCE of 13.15%, J_{sc} of 32.64 mA/cm², V_{oc} of 623 mV, and FF of 64.64% was obtained when DA@G3 (1.5 mg/mL) was incorporated into the solar cell preparation.

Author Contributions: Experimental work, T.C. and H.G.; result evaluation and manuscript preparation, T.C. and J.W.; figure preparing and modification, T.C., L.Y., and A.C.; review and editing, T.S., C.W., and Y.Y. All authors have read and agreed to the published version of the manuscript.

Funding: This research was funded by the Construction Fund of International Joint Research Centre for Optoelectronic and Energy Materials by Yunnan Provincial Department of Finance (No. 20171B033), the Youth Project of Yunnan Province Basic Research Program (202001BB050007), the Yunnan University Action Plan of Serve the Yunnan Province (No. 2016MS15), and the Youth Project of Yunnan Province Basic Research Program (202001BB050006).

Conflicts of Interest: The authors declare no conflict of interest.

References

1. Shiu, S.C.; Chao, J.J.; Hung, S.C.; Yeh, C.L.; Lin, C.F. Morphology Dependence of Silicon Nanowire/Poly(3,4-Ethylenedioxythiophene):Poly(Styrenesulfonate) Heterojunction Solar Cells. *Chem. Mater.* **2010**, *22*, 3108–3113. [[CrossRef](#)]
2. Thomas, J.P.; Leung, K.T. Defect-Minimized PEDOT:PSS/Planar-Si Solar Cell with Very High Efficiency. *Adv. Func. Mater.* **2014**, *24*, 4978–4985. [[CrossRef](#)]
3. Chang, K.W.; Sun, K.W. Highly Efficient Back-Junction PEDOT:PSS /n-Si Hybrid Solar Cell with Omnidirectional Antireflection Structures. *Org. Electron.* **2018**, *55*, 82–89. [[CrossRef](#)]
4. Kou, Y.S.; Yang, S.T.; Thiyagu, S.; Liu, C.T.; Wu, J.W.; Lin, C.F. Solution-Processed Carrier Selective Layers for High Efficiency Organic/Nanostructured-Silicon Hybrid Solar Cells. *Nanoscale* **2016**, *8*, 5379–5385. [[CrossRef](#)] [[PubMed](#)]
5. Zhang, L.; Wang, Z.; Lin, H.; Wang, W.; Wang, J.; Zhang, H.; Sheng, J.; Wu, S.; Gao, P.; Ye, J. Thickness-Modulated Passivation Properties of PEDOT:PSS Layers over Crystalline Silicon Wafers in Back Junction Organic/Silicon Solar Cells. *Nanotechnology* **2019**, *30*, 195401. [[CrossRef](#)]
6. Yoon, S.S.; Khang, D.Y. Ag Nanowire/PEDOT:PSS Bilayer Transparent Electrode for High Performance Si-PEDOT:PSS Hybrid Solar Cells. *J. Phys. Chem. Solids* **2019**, *129*, 128–132. [[CrossRef](#)]
7. He, J.; Hossain, M.A.; Lin, H.; Wang, W.; Karuturi, S.K.; Hoex, B.; Ye, J.; Gao, P.; Bullock, J.; Wan, Y. 15% Efficiency Ultrathin Silicon Solar Cells with Fluorine-Doped Titanium Oxide and Chemically Tailored Poly(3,4-Ethylenedioxythiophene):Poly(Styrenesulfonate) as Asymmetric Heterocontact. *ACS Nano*. **2019**, *13*, 6356–6362. [[CrossRef](#)]
8. Zielke, D.; Pazidis, A.; Werner, F.; Schmidt, J. Organic-Silicon Heterojunction Solar Cells on n-Type Silicon Wafers: The Backpedot Concept. *Sol. Energ. Mat. Sol. C* **2014**, *131*, 110–116. [[CrossRef](#)]
9. Yu, L.; Chen, T.; Feng, N.; Wang, R.; Sun, T.; Zhou, Y.; Wang, H.; Yang, Y.; Lu, Z. Highly Conductive and Wettable PEDOT:PSS for Simple and Efficient Organic/c-Si Planar Heterojunction Solar Cells. *Sol. RRL* **2020**, *4*, 1900513. [[CrossRef](#)]
10. Markose, K.K.; Jasna, M.; Subha, P.P.; Antony, A.; Jayaraj, M.K. Performance Enhancement of Organic/Si Solar Cell Using CNT Embedded Hole Selective Layer. *Sol. Energy* **2020**, *211*, 158. [[CrossRef](#)]
11. Jäckle, S.; Liebhaber, M.; Niederhausen, J.; Büchele, M.; Félix, R.; Wilks, R.G.; Bär, M.; Lips, K.; Christiansen, S. Unveiling the Hybrid n-Si/PEDOT: PSS Interface. *ACS Appl. Mater. Interfaces* **2016**, *8*, 8841–8848. [[CrossRef](#)] [[PubMed](#)]
12. Ouyang, J.; Xu, Q.; Chu, C.W.; Yang, Y.; Li, G.; Shinar, J. On the Mechanism of Conductivity Enhancement in Poly(3,4-Ethylenedioxythiophene):Poly(Styrene Sulfonate) Film through Solvent Treatment. *Polymer* **2004**, *45*, 8443–8450. [[CrossRef](#)]
13. Nam, Y.H.; Song, J.W.; Park, M.J.; Sami, A.; Lee, J.H. Ultrathin Al₂O₃ Interface Achieving an 11.46% Efficiency in Planar n-Si/PEDOT:PSS Hybrid Solar Cells. *Nanotechnology* **2017**, *28*, 155402. [[CrossRef](#)] [[PubMed](#)]
14. He, J.; Gao, P.; Yang, Z.; Yu, J.; Yu, W.; Zhang, Y.; Sheng, J.; Ye, J.; Amine, J.C.; Cui, Y. Silicon/Organic Hybrid Solar Cells with 16.2% Efficiency and Improved Stability by Formation of Conformal Heterojunction Coating and Moisture-Resistant Capping Layer. *Adv. Mater.* **2017**, *29*, 1606321. [[CrossRef](#)] [[PubMed](#)]
15. Jiang, X.; Wang, Z.; Han, W.; Liu, Q.; Lu, S.; Wen, Y.; Hou, J.; Huang, F.; Peng, S.; He, D.; et al. High Performance Silicon–Organic Hybrid Solar Cells Via Improving Conductivity of PEDOT:PSS with Reduced Graphene Oxide. *Appl. Surf. Sci.* **2017**, *407*, 398–404. [[CrossRef](#)]
16. Fang, X.; Song, T.; Liu, R.; Sun, B. Two-Dimensional CoS Nanosheets Used for High-Performance Organic–Inorganic Hybrid Solar Cells. *J. Phys. Chem. C* **2014**, *118*, 20238–20245. [[CrossRef](#)]
17. Pham, V.T.; Hong, P.N.; Hung, T.B.; Hong, N.T.; Van, T.D.; Van, C.N.; Ngoc, M.P. Effect of Surface Morphology and Dispersion Media on the Properties of PEDOT:PSS/n-Si Hybrid Solar Cell Containing Functionalized Graphene. *Adv. Mater. Sci. Eng.* **2017**, *2017*, 2362056.

18. Yang, C.; Sun, Z.; He, Y.; Xiong, B.; Chen, S.; Li, M.; Zhou, Y.; Zheng, Y.; Sun, K. Performance-Enhancing Approaches for the PEDOT:PSS-Si Hybrid Solar Cells. *Angew. Chem. Int. Ed. Engl.* **2019**. [[CrossRef](#)]
19. He, L.; Jiang, C.; Wang, H.; Lai, D.; Rusli. High Efficiency Planar Si/Organic Heterojunction Hybrid Solar Cells. *Appl. Phys. Lett.* **2012**, *100*, 073503. [[CrossRef](#)]
20. Zhang, C.; Zhang, Y.; Guo, H.; Jiang, Q.; Dong, P.; Zhang, C. Efficient Planar Hybrid n-Si/PEDOT:PSS Solar Cells with Power Conversion Efficiency up to 13.31% Achieved by Controlling the SiO_x Interlayer. *Energies* **2018**, *11*, 1397. [[CrossRef](#)]
21. Liu, Y.; Zhang, J.; Wu, H.; Cui, W.; Wang, R.; Ding, K.; Lee, S.T.; Sun, B. Low-Temperature Synthesis TiO_x Passivation Layer for Organic-Silicon Heterojunction Solar Cell with a High Open-Circuit Voltage. *Nano Energy* **2017**, *34*, 257–263. [[CrossRef](#)]
22. Liu, Q.; Khatri, I.; Ishikawa, R.; Fujimori, A.; Ueno, K.; Manabe, K.; Nishino, H.; Shirai, H. Improved Photovoltaic Performance of Crystalline-Si/Organic Schottky Junction Solar Cells Using Ferroelectric Polymers. *Appl. Phys. Lett.* **2013**, *103*, 163503. [[CrossRef](#)]
23. Liu, Y.; Zhang, Z.G.; Xia, Z.; Zhang, J.; Liu, Y.; Liang, F.; Li, Y.; Song, T.; Yu, X.; Lee, S.T.; et al. High Performance Nanostructured Silicon-Organic Quasi p-n Junction Solar Cells Via Low-Temperature Deposited Hole and Electron Selective Layer. *ACS Nano*. **2016**, *10*, 704–712. [[CrossRef](#)] [[PubMed](#)]
24. Zhu, J.; Yang, X.; Sheng, J.; Gao, P.; Ye, J. Double-Layered PEDOT:PSS Films Inducing Strong Inversion Layers in Organic/Silicon Hybrid Heterojunction Solar Cells. *ACS Appl. Energ. Mater.* **2018**, *1*, 2874–2881. [[CrossRef](#)]
25. Uma, K.; Subramani, T.; Syu, H.J.; Lin, T.C.; Lin, C.F. Fabrication of Silicon Nanowire/Poly(3,4-Ethylenedioxythiophene):Poly(Styrenesulfonate)-Graphene Oxide Hybrid Solar Cells. *J. Appl. Phys.* **2015**, *117*, 105102. [[CrossRef](#)]
26. Suhail, A.; Pan, G.; Jenkins, D.; Islam, K. Improved Efficiency of Graphene/Si Schottky Junction Solar Cell Based on Back Contact Structure and DUV Treatment. *Carbon* **2018**, *129*, 520–526. [[CrossRef](#)]
27. Bartolomeo, A.D.; Giubileo, F.; Luongo, G.; Iemmo, L.; Martucciello, N.; Niu, G.; Frasccke, M.; Skibitzki, O.; Schroeder, T.; Lupina, G. Tunable Schottky Barrier and High Responsivity in Graphene/Si-Nanotip Optoelectronic Device. *2D Mater.* **2016**, *4*, 015024. [[CrossRef](#)]
28. Kong, X.; Zhang, L.; Liu, B.; Gao, H.; Zhang, Y.; Yan, H.; Song, X. Graphene/Si Schottky Solar Cells: A Review of Recent Advances and Prospects. *RSC Adv.* **2019**, *9*, 863–877. [[CrossRef](#)]
29. Chen, F.; Xing, Y.; Wang, Z.; Zheng, X.; Zhang, J.; Cai, K. Nanoscale Polydopamine (PDA) Meets pi-pi Interactions: An Interface-Directed Coassembly Approach for Mesoporous Nanoparticles. *Langmuir* **2016**, *32*, 12119–12128. [[CrossRef](#)]
30. Flouda, P.; Shah, S.A.; Lagoudas, D.C.; Green, M.J.; Lutkenhaus, J.L. Highly Multifunctional Dopamine-Functionalized Reduced Graphene Oxide Supercapacitors. *Matter* **2019**, *1*, 1532–1546. [[CrossRef](#)]
31. Hu, X.; Qi, R.; Zhu, J.; Lu, J.; Luo, Y.; Jin, J.; Jiang, P. Preparation and Properties of Dopamine Reduced Graphene Oxide and Its Composites of Epoxy. *J. Appl. Polym. Sci.* **2014**, *131*. [[CrossRef](#)]
32. Qin, S.; Qiu, S.; Cui, M.; Dai, Z.; Zhao, H.; Wang, L. Synthesis and Properties of Polyimide Nanocomposite Containing Dopamine-Modified Graphene Oxide. *High Perform. Polym.* **2018**, *31*, 331–340. [[CrossRef](#)]
33. Huang, J.; Wang, K.; Chang, J.; Jiang, Y.; Xiao, Q.; Li, Y. Improving the Efficiency and Stability of Inverted Perovskite Solar Cells with Dopamine-Copolymerized PEDOT:PSS as a Hole Extraction Layer. *J. Mater. Chem. A* **2017**, *5*, 13817–13822. [[CrossRef](#)]
34. Hou, M.; Zhang, H.; Wang, Z.; Xia, Y.; Chen, Y.; Huang, W. Enhancing Efficiency and Stability of Perovskite Solar Cells Via a Self-Assembled Dopamine Interfacial Layer. *ACS Appl. Mater. Interfaces* **2018**, *10*, 30607–30613. [[CrossRef](#)]
35. Wang, C.; Li, Y.; Zhang, C.; Shi, L.; Tong, S.; Guo, B.; Zhang, J.; He, J.; Gao, Y.; Su, C.; et al. Enhancing the Performance of Planar Heterojunction Perovskite Solar Cells Using Stable Semiquinone and Amine Radical Modified Hole Transport Layer. *J. Power Sources* **2018**, *390*, 134–141. [[CrossRef](#)]
36. Xue, Q.; Liu, M.; Li, Z.; Yan, L.; Hu, Z.; Zhou, J.; Li, W.; Jiang, X.; Xu, B.; Huang, F.; et al. Efficient and Stable Perovskite Solar Cells Via Dual Functionalization of Dopamine Semiquinone Radical with Improved Trap Passivation Capabilities. *Adv. Funct. Mater.* **2018**, *28*, 1707444. [[CrossRef](#)]
37. Xu, F.; Xie, S.; Cao, R.; Feng, Y.; Ren, C.; Wang, L. Prepare Poly-Dopamine Coated Graphene@Silver Nanohybrid for Improved Surface Enhanced Raman Scattering Detection of Dyes. *Sensor. Actuat. B-Chem.* **2017**, *243*, 609–616. [[CrossRef](#)]

38. Lee, W.; Lee, J.U.; Jung, B.M.; Byun, J.H.; Yi, J.W.; Lee, S.B.; Kim, B.S. Simultaneous Enhancement of Mechanical, Electrical and Thermal Properties of Graphene Oxide Paper by Embedding Dopamine. *Carbon* **2013**, *65*, 296–304. [[CrossRef](#)]
39. Kaminska, I.; Das, M.R.; Coffinier, Y.; Niedziolka-Jonsson, J.; Sobczak, J.; Woisel, P.; Lyskawa, J.; Opallo, M.; Boukherroub, R.; Szunerits, S. Reduction and Functionalization of Graphene Oxide Sheets Using Biomimetic Dopamine Derivatives in One Step. *ACS Appl. Mater. Interfaces* **2012**, *4*, 1016–1020. [[CrossRef](#)]
40. Sheng, Z.H.; Zheng, X.Q.; Xu, J.Y.; Bao, W.J.; Wang, F.B.; Xia, X.H. Electrochemical Sensor Based on Nitrogen Doped Graphene: Simultaneous Determination of Ascorbic Acid, Dopamine and Uric Acid. *Biosens. Bioelectron.* **2012**, *34*, 125–131. [[CrossRef](#)]
41. Fan, Q.; Zhang, Q.; Zhou, W.; Xia, X.; Yang, F.; Zhang, N.; Xiao, S.; Li, K.; Gu, X.; Xiao, Z.; et al. Novel Approach to Enhance Efficiency of Hybrid Silicon-Based Solar Cells Via Synergistic Effects of Polymer and Carbon Nanotube Composite Film. *Nano Energy* **2017**, *33*, 436–444. [[CrossRef](#)]
42. Hu, W.; Xu, C.Y.; Niu, L.B.; Elseman, A.M.; Wang, G.; Liu, B.; Yao, Y.Q.; Liao, L.P.; Zhou, G.D.; Song, Q.L. High Open-Circuit Voltage of 1.134 V for Inverted Planar Perovskite Solar Cells with Sodium Citrate-Doped PEDOT:PSS as a Hole Transport Layer. *ACS Appl. Mater. Interfaces* **2019**, *11*, 22021–22027. [[CrossRef](#)] [[PubMed](#)]

Publisher's Note: MDPI stays neutral with regard to jurisdictional claims in published maps and institutional affiliations.



© 2020 by the authors. Licensee MDPI, Basel, Switzerland. This article is an open access article distributed under the terms and conditions of the Creative Commons Attribution (CC BY) license (<http://creativecommons.org/licenses/by/4.0/>).